

The Effects of Anisotropic Insulations with Different Spatial Distributions on Material Properties of Mortar Specimens

Sang-Yeop Chung¹⁾, Mohamed Abd Elrahman^{1,2),*}, and Dietmar Stephan¹⁾

(Received August 25, 2016, Accepted October 23, 2017, Published online December 7, 2017)

Abstract: Insulating concrete is a material designed to reduce heat conduction with pores/insulations, and these pores strongly affect the material characteristics. In general, the insulation effect is directly proportion to the pore volume, while the material strength decreases as the porosity increases. To overcome this contrary, anisotropic insulations with different spatial distributions are proposed and investigated in this study. A set of mortar specimens with different arrangements of coin-shaped insulations are produced to examine the anisotropic insulation effect on the material characteristics. In addition, different types of insulation materials and their effect on the materials are also investigated here. X-ray computed tomography images and probabilistic description methods are used to confirm the arrangement of the insulations. The thermal and mechanical responses for different directions are investigated using both experimental and numerical methods. From the results, it is demonstrated that the use of anisotropic insulations for a specific direction can enhance the insulation efficiently as well as minimizing the loss of compressive strength.

Keywords: insulating concrete, anisotropic insulation, X-ray CT, probability function, thermal conductivity, compressive strength.

1. Introduction

In recent years, energy consumption is considered as a serious problem in many engineering fields, and many efforts have been conducted to improve energy efficiency. Many new buildings and construction materials have been suggested and used over the last decades (Roma-Jr and Martello 2008; Sales et al. 2010; Benmansour et al. 2014). In particular, insulating concrete has been widely used to reduce energy consumption. Insulating concrete is a material designed to enhance insulation effect by using insulating components, such as lightweight aggregates, and entrained pores. The type of insulation contained in the specimen and its characteristics play a significant role in reducing heat transfer and material properties of insulating concrete (Narayanan and Ramamurthy 2000; Baetens et al. 2011; Chabannes et al. 2014; Binici et al. 2016).

Insulating concrete contains numerous pores inside the material, and the volume ratio and the spatial distribution of these insulations strongly affect the characteristics of

concrete. Thus, it is important to correctly investigate the spatial distribution of insulation materials, and many researchers have studied the insulation/pore distribution and its effect on the material properties. Dorey et al. (2002) investigated the pore clustering effect on the material properties of ceramic. Won and Chau (2005) examined the concrete specimens with different constituent distributions. Chung et al. (2013) examined the correlation between the pore characteristics and the directional modulus of lightweight aggregates and evaluated the effect of the pore distribution on thermal properties of insulating specimens using micro-CT images Chung et al. (2016). Hao et al. (2016) investigated the effect of optimized porosity distribution of insulation materials by the variational method.

In general, the thermal conductivity decreases as the volume ratio of insulations increases, while the mechanical properties, such as strength and directional modulus, have a direct proportion to the insulation volume. In order to overcome the contrary behavior between these physical properties, several studies have been reported on related methods. Cabrillac and Malou (2000) proposed the modeling of anisotropic pores using a homogenization method, and Zake-Tiluga et al. (2014) investigated anisotropic behavior of compressive strength in porous ceramics. In particular, Cabrillac et al. (2006) suggested and examined concretes with anisotropic pores and their effect on the mechanical properties. Chung et al. (2016) also investigated the effect of ellipsoidal (anisotropic) pores on the thermal properties of materials using 3D printed samples. From these studies, it is demonstrated that a proper use of anisotropic

¹⁾Building Materials and Construction Chemistry, Technische Universität Berlin, Gustav-Meyer-Allee 25, 13355 Berlin, Germany.

*Corresponding Author; E-mail: mohattia76@gmail.com

²⁾Structural Engineering Department, Mansoura University, Elgomhouria St., Mansoura City 35516, Egypt.

pores can effectively overcome the contrary responses between thermal and mechanical properties without causing performance losses.

However, pores with anisotropic geometries are difficult to produce in a real specimen due to heterogeneity of concrete. Thus, rigid insulation materials with very low thermal conductivity can be used as artificial pores to examine the effect of anisotropic pores on the characteristics of insulating concrete. Several materials have been used as insulation materials; Gunduz (2008) used pumice aggregates as an insulation materials to investigate the effect on thermal properties and showed its effect in reducing the thermal conductivity, and Ng and Low (2010) investigated the thermal properties of specimens with newspaper sandwiched lightweight panels, which is much lower than that of conventional concrete. Jiang et al. (2013) adopted several natural leaves to improve the insulation of concrete by reducing energy consumption and environmental damage.

In this study, three different materials are utilized as insulation materials for the specimens: low-density expanded polystyrene (EPS), Af/Armaflex (Armacell, UK) made of elastomeric nitrile rubber, and corrugated paper used for packing box; these materials have very low thermal conductivity and can be utilized as alternative pores. To secure anisotropic pores (or insulations) in the sample, these three insulation materials were cut into a coin-shape, and a set of insulating mortar specimens with the coin-shaped insulations were generated to evaluate the effect of anisotropic pores on the material characteristics and properties. Using these artificial anisotropic insulations, the real samples with anisotropic pores can be produced, and their arrangements can be easily controlled. For characterization of the insulation distributions, probability functions, such as two-point correlation (Tewari et al. 2004; Gokhale et al. 2005) and lineal-path functions (Lu and Torquato 1992; Chung and Han 2010), were used. These probability functions were utilized to describe the degree of pore clustering and connectivity for a specific direction (Ke et al. 2009; Neithalath et al. 2010). Effects of anisotropic insulations on the material properties were examined experimentally and numerically.

The main objective of this study is to examine the effect of the spatial distribution of different anisotropic insulations on the physical properties of mortar specimens. For the purpose, different insulation materials were used to secure anisotropic artificial pores in the specimens. In addition, the effects of the insulation volumes and the spatial distribution of insulations on the insulating specimens were also investigated. For effective modeling of the specimens with anisotropic insulations, virtual insulating specimens with different distributions of insulations were generated, and their characteristics and properties were numerically computed. Then, a set of concrete (mortar) specimens with different insulations and arrangements were produced based on the numerical results. The insulation arrangements within the concrete specimens were confirmed using X-ray computed tomography (CT) without damaging the specimen. The material properties, such as the thermal conductivity, compressive strength, and Young's modulus, were also evaluated from experimental methods.

The thermal properties of the insulating specimens are examined using a Hot Disk, a device which satisfies ISO standard (22007-2) DeutscheNorm (2012). The compressive strength values of the specimens were measured using a Toni Technik loading tool DeutscheNorm (2010). The obtained properties were compared with those from simulations. The relationship between the probabilistic descriptions and the physical properties is investigated to evaluate the effect of anisotropic insulations on the material characteristics of insulating mortar specimens.

2. Concrete Specimens with Different Anisotropic Insulations

A set of virtual samples with different insulation distributions are designed to identify the effect of anisotropic insulations on the characteristics and properties of materials. Then, real mortar specimens with different insulation types and distributions are manufactured, and their properties as well as the spatial distribution of insulations are also investigated.

2.1 Modeling of Virtual Samples with Different Insulation Distributions

Here, a set of virtual samples with different number of anisotropic insulations are generated. For a geometry of anisotropic insulation, Cabrillac et al. (2006) and Chung et al. (2016) reported that an ellipsoid is an optimal shape for the anisotropic insulation; however, ellipsoidal insulations are difficult to produce for a real specimen. Therefore, all the insulation materials here are alternatively designed as coin-shape.

Figure 1 shows target virtual specimens with different numbers of anisotropic insulation layers. Each side of the virtual samples in Fig. 1 is discretized into 150 voxels for the x , y , and z directions, and each sample is composed of total of 3,375,000 voxels. All the coin-shape insulations have the same dimension with diameter of 0.16 and thickness of 0.032 in a unit cube with edge length 1, and each insulation layer in the x - y plane is composed of 25 anisotropic insulations (5×5 in $x \times y$ direction). The virtual specimens in Fig. 1 are denoted as L3 (Fig. 1a), L6 (Fig. 1b), and L9 (Fig. 1c) samples. Each specimen contains 3 (L3), 6 (L6), and 9 (L9) insulation layers with total of 75, 150, and 225 coin-shaped insulations, respectively. The volume ratios of anisotropic insulations in each specimen are 5.97% (L3), 9.29% (L6), and 13.27% (L9). Using these samples, the effect of the anisotropic insulations with different spatial distributions can be examined numerically.

2.2 Preparation of the Mortar Specimens with Different Anisotropic Insulations

The designed specimens in Fig. 1 are produced as real mortar specimens with different types of insulations. For the purpose, three different materials are used for insulations: expanded polystyrene (EPS), Af/armaflex (Armacell, UK), and corrugated paper; these insulation materials are denoted

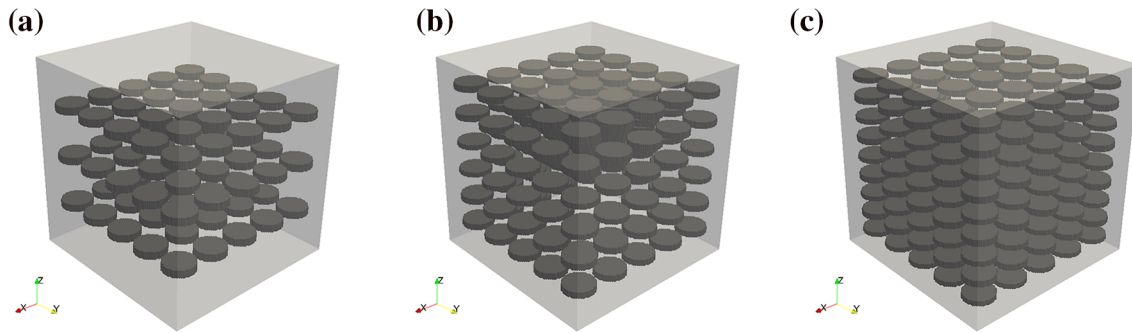


Fig. 1 Virtual specimens with different arrangements of anisotropic insulations: **a** L3 sample with 3 insulation layers (total of 75 insulations), **b** L6 sample with 6 layers (150 insulations), **c** L9 samples with 9 layers (225 insulations) [In the figure, the dark gray voxels represent anisotropic insulations. Each coin-shaped insulation has the same dimension, and each insulation layer is composed of 25 insulations (5 × 5 in xy plane)].

here as EPS, Rubber, and Paper, respectively. These insulations are selected because of their low thermal conductivity and formability, and the physical characteristics of each insulation material are shown in Table 1; these properties are obtained from experimental devices and other investigators including the manufacturers (Yucel et al. 2003; Russ et al. 2013).

Figure 2 shows the preparation of the mortar specimens with different anisotropic insulations. All the insulations are cut into coin-shaped pieces with diameter of 16.0 ± 1.0 mm and thickness of 3.0 ± 1.0 mm. The mortar specimens are prepared in a mold with dimensions of $100 \times 100 \times 100$ mm. To produce regular arrangement of the insulations, a layer with a specific thickness is spread in the mold. Then, the coin-shaped insulations are uniformly distributed as shown in Fig. 2, and repeat the same procedure by considering the target number of insulation layers. The thickness between each insulation layer depends on the total number of layers in the specimen; the layer thicknesses of the specimens with 3, 6, and 9 insulation layers are 24.0, 12.8, and 8.3 mm, respectively. The whole process is repeated until the entire specimen is filled with mortar along the height direction. The mix designs are given in Table 2, and CEM I 42.5N is used for all specimens. The used aggregates in this study are normal sand with size fraction of 0–2 mm. Using these specimens, the effects of the insulation distributions as well as the type of insulations on the material properties are investigated.

3. Characterization and Property Measurements of Anisotropic Insulations

3.1 Probabilistic Characterization of Anisotropic Insulations

The insulation distributions in the specimens significantly affect the material properties of insulating concrete. For more detailed investigation of the spatial distribution of insulations, appropriate quantitative and qualitative methods are required. Here, low-order probability functions, such as two-point correlation and lineal-path functions, are used to examine the anisotropic insulation distribution, and their integrations are also utilized for the quantitative description.

3.1.1 Two-Point Correlation Function

Among the several probability functions, the two-point correlation function, denoted as $P_{ii}(r, \theta, \phi)$, is adopted. $P_{ii}(r, \theta, \phi)$ is the probability that any two points are located in the insulation phase Tewari et al. (2004) and utilized to describe the degree of phase clustering for a specific direction. Here, i denotes the insulation phase, r is the distance between two points, θ is the angle between a test line and the z -axis, and ϕ is the angle between the projection of a test line on the xy -plane and the x -axis. For two-phase materials that are classified into insulations and solids, the general limits of the two-point correlation function for the insulation phase are given as follows (Gokhale et al. 2005; Kumar et al. 2006):

Table 1 Physical properties of insulation materials.

Types	Mortar	EPS	Rubber	Paper
Thermal conductivity (W/m/K)	1.835	0.029	0.033	0.050
Density (kg/m ³)	1841	16	20	70
Specific heat (J/g/K)	850	1300	1500	361
Elastic modulus (GPa)	20	0.2	0.1	0.6
Poisson's ratio	0.2	0.3	0.42	0.05
Yield strength (MPa)	80	0.1	0.2	0.4

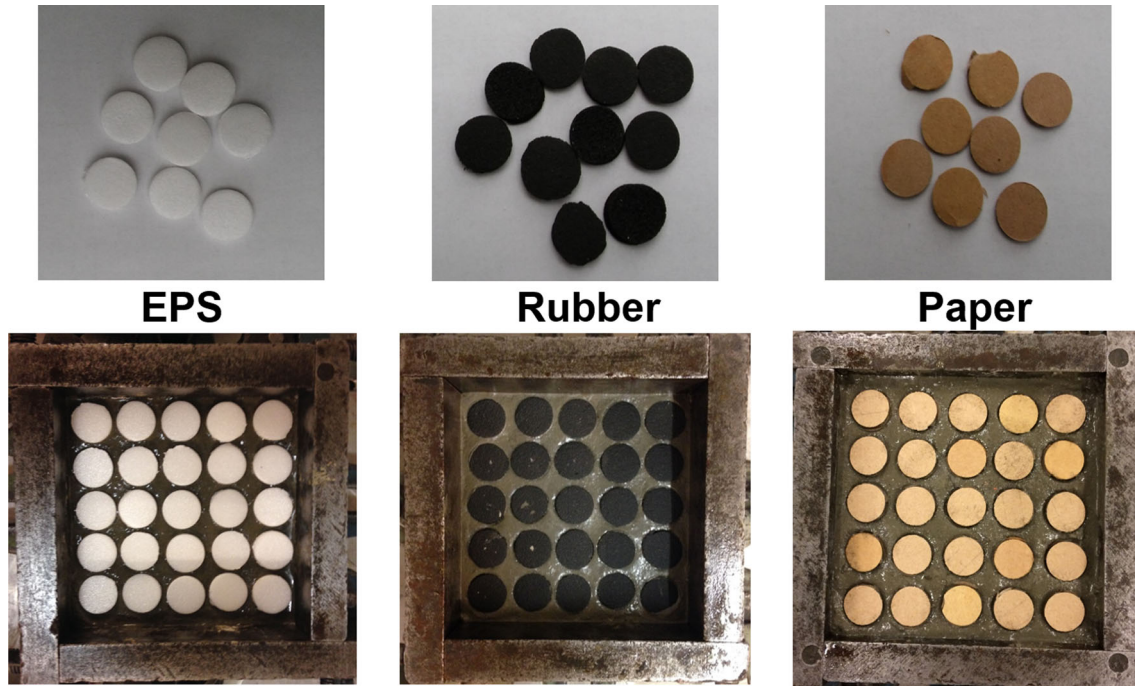


Fig. 2 Insulating specimens with different anisotropic insulation materials.

Table 2 Mix design for the mortar specimens in Fig. 2.

Specimens	Reference	EPS specimen	Rubber specimen	Paper specimen
Cement (g)		750		
Sand (g)		1500		
Water (g)		375		
W/C ratio		0.5		
EPS (layer)	–	3/6/9 layers	–	–
Rubber (layer)	–	–	3/6/9 layers	–
Paper (layer)	–	–	–	3/6/9 layers

$$\lim_{r \rightarrow 0} P_{ii}(r, \theta, \phi) = f_i, \quad \lim_{r \rightarrow \infty} P_{ii}(r, \theta, \phi) = [f_i]^2 \quad (1)$$

where f_i is the volume fraction of the insulation phase. In Eq. (1), the probability of finding the insulation phase at both points converges to f_i as the distance between two points approaches zero, while the function converges to the product of f_i as r increases. P_{ii} , can be calculated using a simple form of the function suggested by Gokhale et al. (2005) as:

$$P_{ii}(r, \theta, \phi) = f_i(1 - f_s[1 - \exp\{-([P_L(\theta, \phi)]_{is}/(2f_i f_s))r\}]) \quad (2)$$

where the subscript s denotes the solid phase, f_s is the solid volume fraction, and $[P_L(\theta, \phi)]_{is}$ is the number of intersections between a test line and the i - s phase interface per unit test line length.

The two-point correlation function can be utilized to describe the spatial distribution of insulations in materials;

however, it is difficult to be used for quantitative analysis because the function is a form of the probability distribution function (Chung et al. 2013, 2016). To describe the probabilistic function as a representative value, P_{ii} for a particular direction is integrated from 0 to 1, and normalized by dividing the insulation volume fraction of the specimen. Here, the integration of the function is expressed as $\overline{P_{ii}}$ and calculated as follows:

$$\overline{P_{ii}} = \frac{1}{f_i} \int_0^1 P_{ii} d\bar{r} \quad (3)$$

where \bar{r} denotes r / D , and D is the specimen length. For the quantitative description of the insulation distributions, $\overline{P_{ii}}$ values for different directions are calculated and assigned to each point of a grid represented on a sphere, which is composed of 1538 nodal points. Here, the 3D space is discretized into 1538 grids for effective visualization of anisotropy, and the calculation of \bar{r} is repeated for the whole discrete directions. The $\overline{P_{ii}}$ values between the nodal points

are calculated from the standard finite element interpolation, and detailed description of this method is shown in (Chung et al. 2013; Han and Dawson 2005).

3.1.2 Lineal-Path Function

The lineal-path function, $L_i(r, \theta, \phi)$, is also used here to describe the continuity of insulations. $L_i(r, \theta, \phi)$ is the probability that a randomly placed line with length r is located in the insulation phase Chung et al. (2016). Unlike $P_{ii}(r, \theta, \phi)$, $L_i(r, \theta, \phi)$ can be utilized to examine the continuous connectivity of the insulation phase for a specific direction because the function only includes the case that a whole line is positioned in the insulation phase Lu and Torquato (1992); therefore, $L_i(r, \theta, \phi)$ can be utilized as a complementary function of $P_{ii}(r, \theta, \phi)$. The general limits of $L_i(r, \theta, \phi)$ are given as:

$$\lim_{r \rightarrow 0} L_i(r, \theta, \phi) = f_i, \quad \lim_{r \rightarrow \infty} L_i(r, \theta, \phi) = 0 \quad (4)$$

In this study, the Coker and Torquato's method is adopted to obtain $L_i(r, \theta, \phi)$ for the insulating specimens, and detailed procedure is presented in Coker and Torquato (1995). Likewise the case of $P_{ii}(r, \theta, \phi)$, $L_i(r, \theta, \phi)$ for different directions are also integrated and normalized for quantitative description of the insulation distribution, as follows:

$$\bar{L}_i = \frac{1}{f_i} \int_0^1 L_i d\bar{r} \quad (5)$$

To quantify the anisotropy of the insulation distribution, \bar{L}_i values for different directions are calculated.

3.2 Investigation of the Physical Properties of the Specimens

The thermal and mechanical properties of the specimens with different insulations and distributions are examined using numerical as well as experimental methods. The material responses of the virtual samples are evaluated to investigate the anisotropy of the properties using finite element (FE) analysis. In addition, the thermal conductivity and compressive strength values of the specimens with different types of insulations are examined using experimental tools.

3.2.1 Numerical Simulation for Thermal and Mechanical Analysis

To investigate the anisotropic effect on the material properties, the thermal and mechanical responses of the virtual samples in Fig. 1 are evaluated using FE simulations. The ABAQUS package ABAQUS (2013) is used for the numerical simulations, and detailed descriptions on the FE formulations for thermal and mechanical analysis are in (Chung et al. 2016; Incropera et al. 2006); only a brief description is presented here.

For heat transfer analysis, the governing equation for 3D heat flow by considering heat loss can be described as:

$$\frac{\partial T}{\partial t} = \frac{k}{\rho C} \left(\frac{\partial^2 T}{\partial x^2} + \frac{\partial^2 T}{\partial y^2} + \frac{\partial^2 T}{\partial z^2} \right) - \lambda \cdot T^* \quad (6)$$

where, ρ is the mass density (kg/m^3), C is the specific heat (J/g/K), and k is the thermal conductivity (W/m/K). T is the temperature (K), T^* is the surrounding temperature (K), λ is the heat loss coefficient ($1/\text{s}$), and t is the time (s).

For the FE simulation, a weak form is obtained by integrating the governing equation in Eq. (6), and the heat flux can be calculated by averaging the specimen heat flux. Then, the effective thermal conductivity is calculated by the Fourier law as:

$$k_{(n)} = \frac{q_{(n)} L}{\Delta T_{(n)}} \quad (7)$$

where $\Delta T_{(n)}$ is the temperature difference in the direction of thermal conduction, n is the directional component, and L is the characteristic length.

The required input parameters for the heat analysis, such as the bulk thermal conductivity and specific heat of hydrated mortar and insulation materials, are obtained from experiments using a Hot Disk device that satisfies ISO standard (22007-2) DeutscheNorm (2012); the parameters used here are presented in Table 1. For the boundary condition, a constant temperature (60°C) is imposed on the top side of the specimen, while heat loss is allowed only in the opposite side along in each direction. The remaining surfaces are considered to have no heat loss, and the surrounding temperature is set as 22°C . Heat loss coefficient, λ , is obtained from the Hot Disk device and selected as $1.6 (1/\text{s})$. In this study, the thermal conductivities for all the specimens are measured in the x and z directions to examine anisotropic thermal properties.

The compressive strengths of the virtual samples are also evaluated using the FE analysis. For the simulations, the ABAQUS software including the concrete damage plasticity (CDP) model is used to describe the behavior of the virtual insulating specimens with different insulation distributions. Detailed descriptions of the FE formulations are presented in Kmiecik and Kaminski (2011), and only a brief description of the constitutive model is shown in this paper. The stress-strain relation of the CDP model is governed by a scalar damaged elasticity as:

$$\sigma = (1 - d) \mathbf{D}_0^{el} : (\epsilon - \epsilon^{pl}) = \mathbf{D}_0 : (\epsilon - \epsilon^{pl}) \quad (8)$$

where, σ is the stress tensor, d is the scalar stiffness degradation variable between 0 (undamaged material) to 1 (fully damaged material), \mathbf{D}_0^{el} is the initial elastic modulus, \mathbf{D}_0 is the degraded elastic stiffness, ϵ is the total strain tensor, and ϵ^{pl} is the plastic strain tensor.

Each elemental stress is calculated at the center of each element, and the effective stress is obtained from the element stresses by integrating over the whole volume. For the boundary condition, a displacement boundary condition is imposed on the top surface in each x and z direction, while a fixed boundary condition is applied to the bottom plane. Other remaining lateral surfaces are set to be traction free. The parameters for the CDP model, such as dilation angle and eccentricity, are selected and adjusted from the data

in (Kmiecik and Kaminski 2011; Jankowiak and Lodygowski 2008). The input parameters for the mechanical simulations of the specimens with different insulations are listed in Table 1. The simulation results are compared with experiments for validation purpose. The effect of different insulations and the correlation between the insulation distribution and the directional compressive strength are also confirmed from the results

3.2.2 Experiments for the Evaluation of Material Properties

Using the Hot Disk machine (Hot Disk AB, Sweden), thermal properties, such as thermal conductivity, thermal diffusivity, and specific heat capacity can be effectively measured, and the obtained results are utilized for the numerical simulations as the input parameters. This device is based on the use of a transiently heated plane sensor, and the sensor is sandwiched between two sheets of an insulating material to be measured. Detailed description of the measurement process is shown in Fig. 3a. The compressive strength of the specimens are also evaluated using the Toni Technik (Zwick Roell, Germany) machine in Fig. 3b, a device which meets German standard 12390-4 Deutsche-Norm (2010) with loading rate of 0.50 MPa/s and with loading capacity of 3000 kN. Likewise the thermal property, the strengths of the specimens are evaluated for the different (x and z) directions to confirm the effect of anisotropic insulations on the mechanical properties of the specimens. All tests have been carried out on three specimens and the mean value is considered in each case. Here, at least three specimens of each case are tested to enhance the accuracy, and only the mean values are presented.

4. Characteristics and Properties of the Insulating Specimens with Different Anisotropic Insulations

The characteristics of the insulation distributions are described using the methods in Sect. 3.1 In particular, the anisotropic characteristics of the specimens with different insulation distributions are identified, and their effects on the

material properties are examined using the numerical and experimental methods.

4.1 Anisotropic Characteristics of the Virtual Insulating Specimens

The virtual specimens in Fig. 1 contain anisotropic insulations inside the specimens. The characteristics of the insulation distributions are investigated using the probabilistic and quantitative methods. Fig. 4 shows the probability functions of the virtual samples with anisotropic insulations in the x , y , and z directions; Fig. 4a–c are the two-point correlation function ($P_{ii}(r)$), and Fig. 4d–f are the lineal-path function ($L_i(r)$). In each function, r represents the distance between two random points, and D is the specimen edge length. In these figures, the porosities and the directional characteristics of the insulation distributions are clearly described; the porosities in each function are 0.0597, 0.0929, and 0.1327 for L3, L6, and L9 samples, respectively. $P_{ii}(r)$ and $L_i(r)$ in Fig. 4 show almost the same functions in the x and y directions, while the function values in the z direction are smaller than other directions; this represents that the size of the insulations in the z -direction is smaller than that of other directions, and the insulation distributions in the specimens are anisotropic. In Fig. 4a–c, the relative degree of clustering of insulations can be estimated using $P_{ii}(r)$. In particular, $L_i(r)$ can be used to demonstrate the anisotropy of the coin-shaped insulation used in this study. The ratio between the diameter and the thickness of each coin-shaped insulation is designed as approximately 5:1. In Fig. 4d–f, the function values in the x and y directions are zero when r / D reaches 0.16, while the function for the z -direction is zero when r / D is about 0.3; this ratio is almost identical with that of the coin-shaped insulation, and it is examined that the probability functions used here can be effectively used to describe the directional characteristics of insulation materials.

For the quantitative description of the insulation distribution, $\overline{P_{ii}}$ of the specimens in Fig. 1 is also investigated. To describe the relative anisotropy of the insulation distribution, $\overline{P_{ii}}$ for every direction is divided by the minimum value of $\overline{P_{ii}}$ for each specimen, and the $\overline{P_{ii}}$ values are visualized on a sphere mesh, as shown in Fig. 5. In these figures, the indexed values ($\overline{P_{ii}}/\min\overline{P_{ii}}$) for the x - y plane is distinctly larger than that of the z -direction. The maximum anisotropy

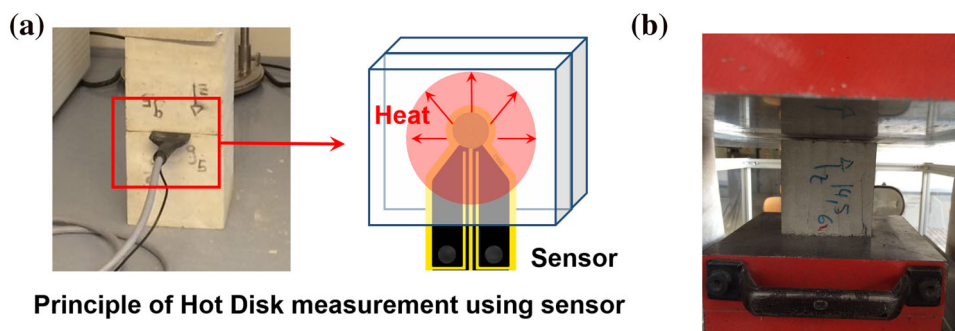


Fig. 3 The use of the devices for evaluating material properties: a Hot Disk device and its operation principle, b Compressive strength evaluation.

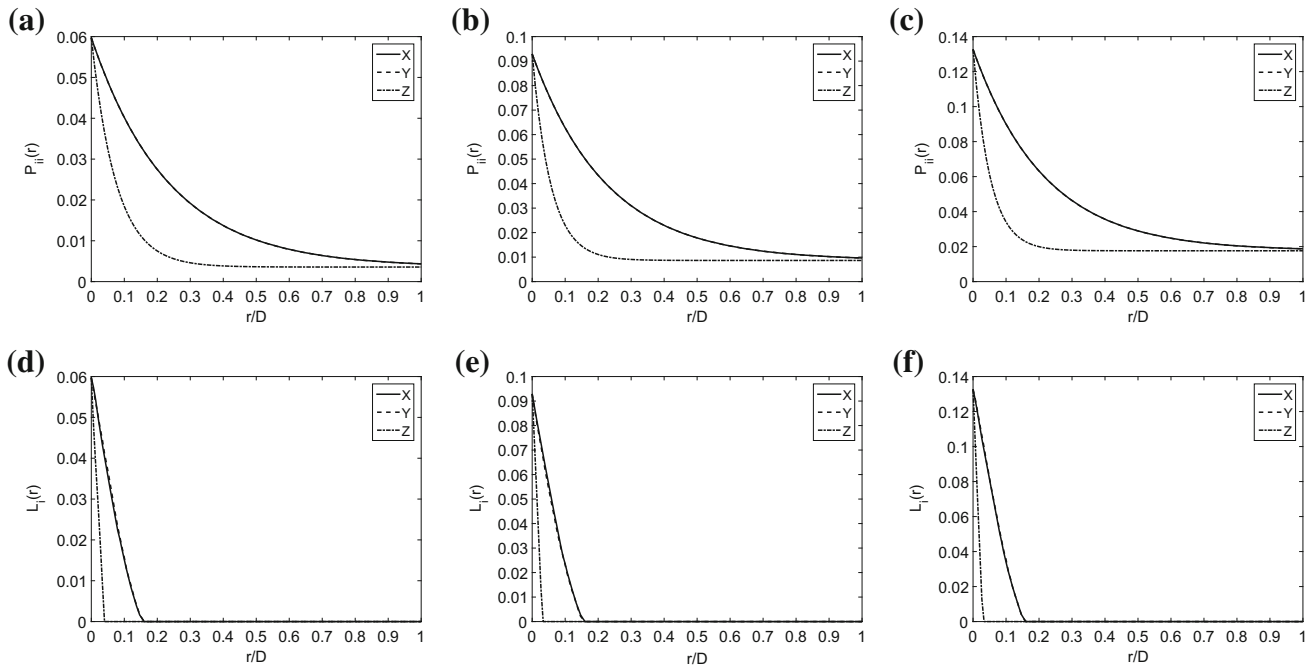


Fig. 4 Probability functions of the specimens: **a** $P_{ii}(r)$ for L3 sample, **b** $P_{ii}(r)$ for L6 sample, **c** $P_{ii}(r)$ for L9 sample, **d** $L_i(r)$ for L3 sample, **e** $L_i(r)$ for L6 sample, **f** $L_i(r)$ for L9 sample (Note D is the edge length of the sample, and r is the distance between two points.).

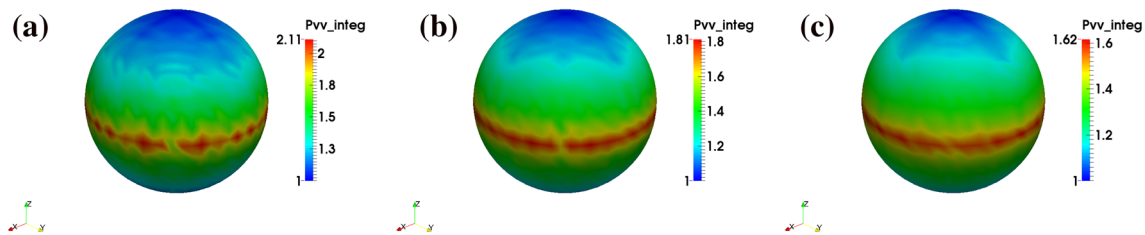


Fig. 5 The spatial distribution of the integrated $P_{ii}(r)$ ($\overline{P_{ii}}$) for the insulation specimens: **a** L3 sample, **b** L6 sample, **c** L9 sample (Note The values on colorbar represent the relative anisotropy for each direction.).

ratio of $\overline{P_{ii}}$ between different directions decreases as the number of insulation layers for the z -direction increases: 2.11 (L3), 1.81 (L6), and 1.62 (L9). In addition, the anisotropy ratio of the integration of $L_i(r)$, $\overline{L_i}$, bears the same characteristics, as 4.5 (L3), 4.2 (L6), and 3.3 (L9), although they are not visualized here. The maximum anisotropy ratio decreases as the total volume of the insulations increases because the insulation layers are stacked only in the z -direction. These results demonstrate that $\overline{P_{ii}}$ as well as $\overline{L_i}$ can be efficiently utilized to describe the characteristics of the insulation distributions, and the insulation distributions in each specimen are anisotropic.

4.2 Material Responses of the Virtual Insulating Specimens

The thermal and mechanical properties of the virtual specimens with different insulation types and distributions are investigated using FE simulations. Fig. 6 shows the contours of heat flux and temperature isosurfaces for the virtual insulating specimens with Rubber insulations. In the heat flux contours (Fig. 6a, c, and e), it can be confirmed that

heat flows through a solid (mortar) part, while heat transfers rarely through insulation parts. In particular, the heat transfers well through the x -direction, the direction parallel to the flat surface of the coin-shaped insulation; however, the less heat flows through the z -direction than other (x and y) directions because the flat surfaces of the coin-shaped insulations disrupt the heat flow. In all directions, the solid region where heat transfers mostly, decreases as the volume of insulations increases; therefore, the total amount of heat which flows through the solids decreases as more coin-shaped insulations are contained in the specimen. The effect of the coin-shaped insulations can be also identified from the temperature isosurfaces in Fig. 6b, d, and f. In the isosurfaces for the x -direction, the isosurfaces are almost flat because the insulations parallel to the heat flow direction rarely affect the heat transfer. However, in the right figures of Fig. 6b, d, and f, the fluctuations of the temperature isosurfaces can be found near the insulations; this result demonstrates that the coin-shaped insulation strongly affects the hear flow for the perpendicular direction to its flat surface. The same trends are also examined for the use of different insulations, such as EPS and Paper.

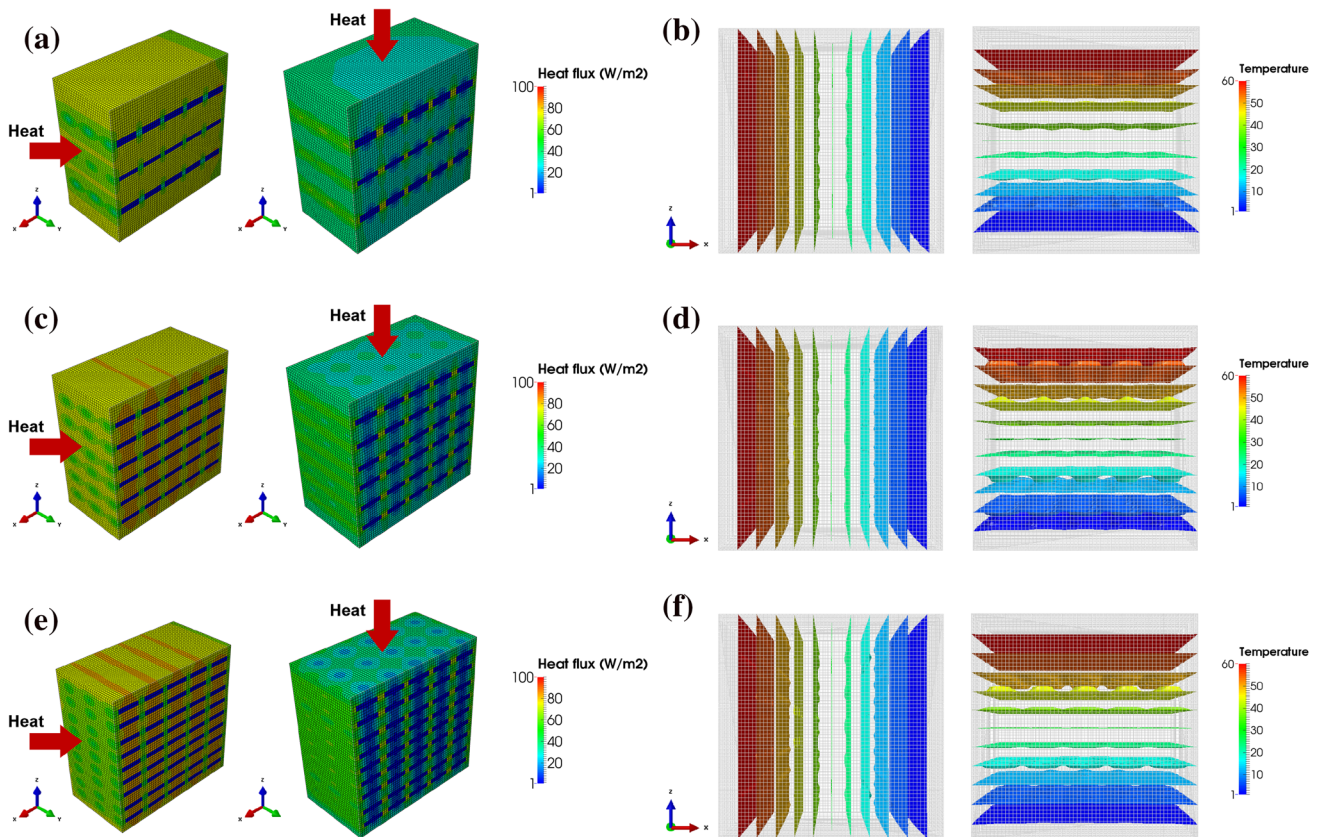


Fig. 6 The view cut of heat flux contour and temperature isosurface of the specimens with Rubber insulations for the x and z directions: **a** Heat flux of L3 sample, **b** Temperature isosurface of L3 sample, **c** Heat flux of L6 sample, **d** Temperature isosurface of L6 sample, **e** Heat flux of L9 sample, **f** Temperature isosurface of L9 sample (*Note* In all figures, left figure is for the x -direction heat flow, and right figure is for the z -direction heat flow.).

The mechanical responses of the virtual specimens with Rubber insulations are also investigated using FE analysis. Fig. 7 shows the stress contours of the specimens with anisotropic insulations. In the contour figures, the effect of coin-shaped insulations can be identified. In the left figures of Fig. 7, the stress distributions are relatively uniform over the whole specimen when the loading is applied to the direction that parallel to the flat surfaces of the coin-shaped insulations (x -direction), although the vicinity of the insulations shows less stress values than other parts. In contrast, when the loading is applied to the z -direction, perpendicular to the flat surface of the anisotropic insulation, the stress concentrations can be found near the edge and vertex of the coin-shaped insulations, and these stress concentrations can be critical for early specimen failure from that location; it denotes that the direction of coin-shaped (anisotropic) insulations affects the mechanical responses of the specimen significantly. Likewise the thermal responses, the same tendencies of the stress distribution are confirmed for the different insulation materials.

For the quantitative investigation of the material responses, thermal conductivity and compressive strength are calculated from the simulation results in Figs. 6 and 7, as shown in Fig. 8. In Fig. 8a, the thermal conductivities of the virtual specimens with different insulation distributions are presented. For all insulation materials, the thermal conductivity as well as compressive strength decrease as the number

of insulation layers increases. In particular, both material properties in the z -direction significantly decrease more than those of the x -direction as the layer number increases. From these results, as shown in Figs. 6 and 8, it is confirmed that the material properties are more affected by the coin-shaped insulations in the perpendicular direction to the flat surface of the insulation. The effect of the different insulations can also be examined from the graphs; the use of different insulations rarely affects the thermal and mechanical properties for the x -direction, as shown in Fig. 8. Otherwise, the material properties for the z -direction are affected by the type of insulation, especially the compressive strength of the specimen. In these results, it is shown that the EPS is the most effective to reduce the thermal conductivity because of its higher specific heat Owrak et al. (2015), while corrugated paper is the most beneficial insulation material for larger strength of the specimen because of its larger elasticity and strength. Fig. 8 is the theoretical result to investigate the effect of different insulations and distributions on material characteristics and properties.

4.3 Physical Properties of the Insulating Specimens with Different Anisotropic Insulations

Here, experimental study is also performed to investigate the effect of anisotropic insulations on the real specimens. Fig. 9 shows the thermal conductivity and compressive

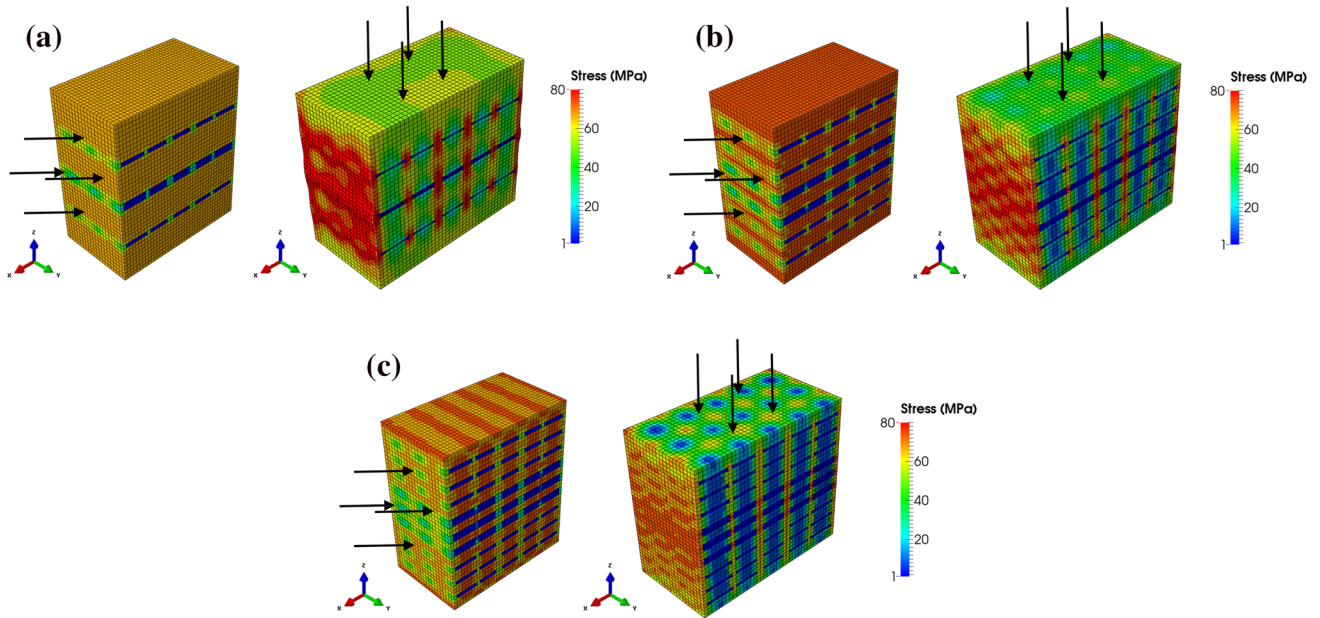


Fig. 7 The view cut of von-Mises stress contour of the specimens with Rubber insulations for the x and z directions: **a** L3 sample, **b** L6 sample, **c** L9 sample (Note: In the figures, left figure is for the x -direction of loading, and right figure is for the z -direction of loading.)

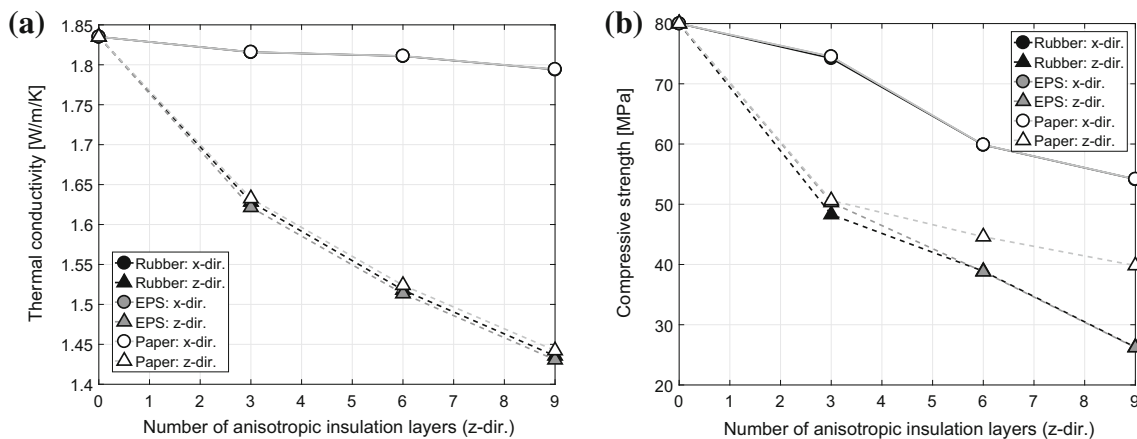


Fig. 8 Comparison of numerical material properties of the virtual insulating specimens with different insulations for the x and z directions: **a** Thermal conductivity, **b** Compressive strength.

strength of the real mortar specimens with anisotropic insulations measured from experimental tools. For the property evaluation, the Hot Disk (thermal) and the Toni Technik (mechanical) devices are used here. For each case, measurements are repeated at least 6 times in order to improve accuracy. The mean values are calculated by excluding the extreme values, and the difference between the used values are within 3%. In Figs. 8 and 9, the differences between the numerical and experimental results of the material properties can be identified; the differences are generally within 7%, and this error level can be considered as a reasonable tolerance. In Fig. 9, it is confirmed that both thermal conductivity and compressive strength decrease as the insulation volume increases, like the simulation results. In general, compressive strength and directional modulus of materials decrease as the weight of the specimen decreases,

while the insulation effect increases; the results in Fig. 9 demonstrate the effect of the weight loss of the specimen on the material properties, and the anisotropic insulation can be utilized to optimize this phenomenon. In the experimental results, the anisotropic trends of material properties are similar to those of the simulations, while the differences between the different types of insulations are more distinct than the simulations; these differences are mainly due to the coarse structure of the insulations which can be filled by mortar in the real specimens and are not considered in the simulation model. In addition, the location movements of the insulations can also affect the difference between the simulation and the experiment. Fig. 10 shows the partial sections of X-ray CT images for each specimen. In this figure, it is examined that the coin-shaped insulations are positioned well as originally designed, but some position shifts and

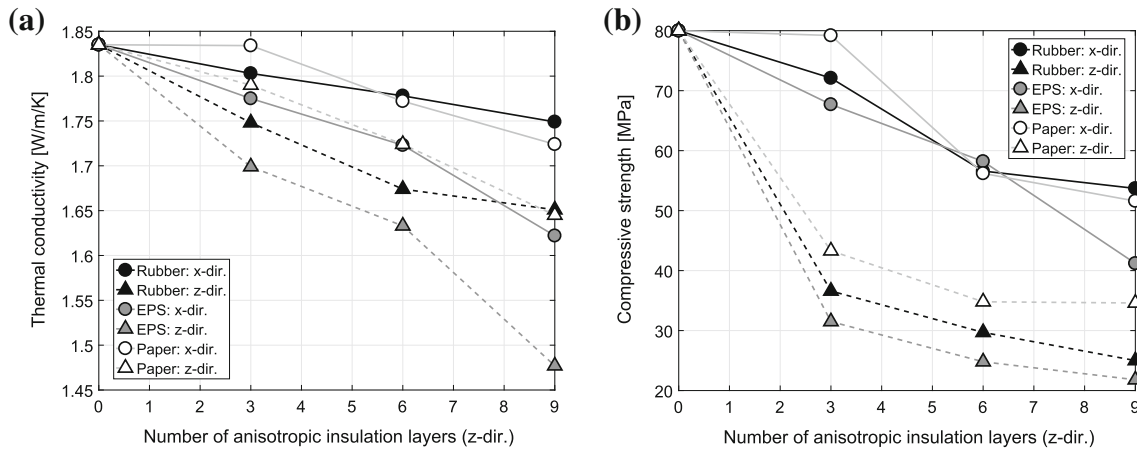


Fig. 9 Comparison of experimental material properties of the insulating specimens with different insulations for the x and z directions: **a** Thermal conductivity, **b** Compressive strength.

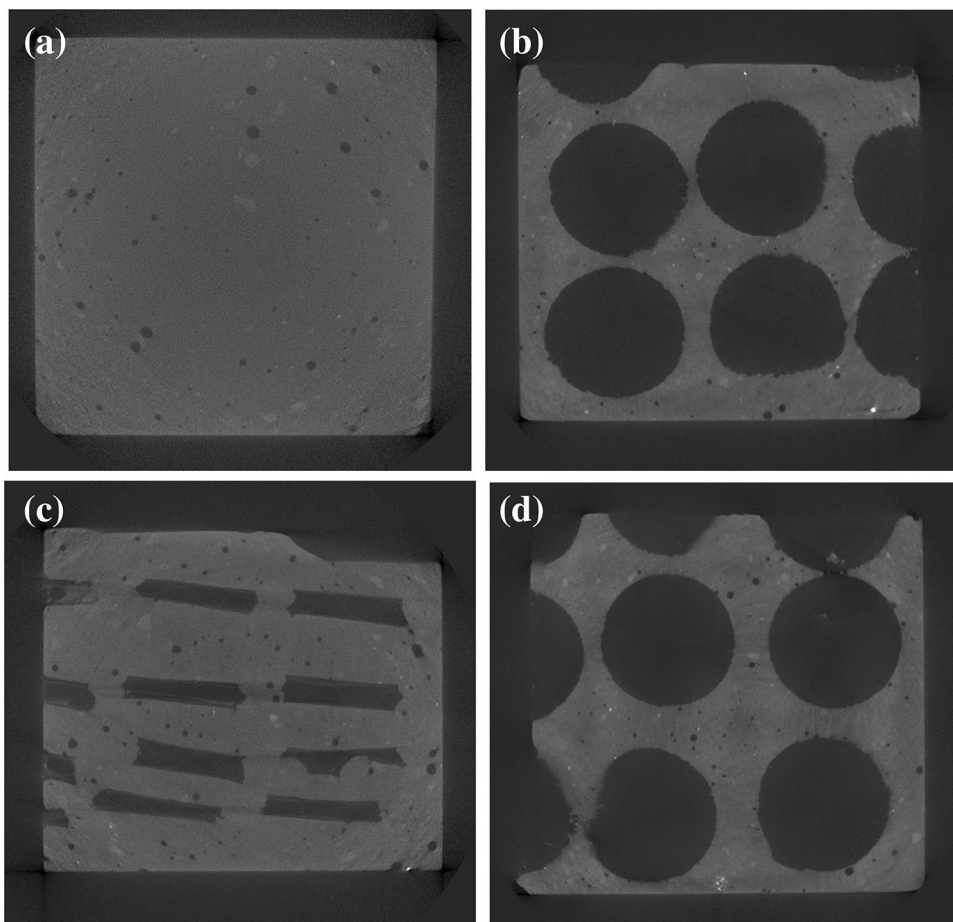


Fig. 10 X-ray CT images of the insulating specimens with coin-shaped insulations: **a** Reference, **b** Rubber specimen, **c** Side view of Paper specimen, **d** EPS specimen (*Note* In these figure, only a quarter of the section image is visualized due to the limitation of image resolution.).

irregular shapes of the insulations which occurs during the sample preparation can be found. In addition, it can be seen in Fig. 10c that mortar is infiltrated into the corrugated paper in some layers; these migrated and infiltrated insulations can cause the differences between the results. Even though the differences, the general trend of the thermal and mechanical

characteristics of the mortar specimens with anisotropic insulations is almost the same with that of the simulations. Likewise the numerical results, EPS is the most effective material to have the lower thermal conductivity, and Paper can be considered as a material to obtain larger strength than other materials used here. The results suggest that the use of

anisotropic insulations can improve the material's insulation effect, especially when heat flows through the perpendicular direction to the flat surface of the anisotropic insulation, and arrangements and types of insulation materials should be appropriately considered.

5. Conclusions

The anisotropic insulation and its effect on the material characteristics are examined. To secure anisotropic insulations in the specimen, a set of coin-shaped insulations with different materials, such as expanded polystyrene (EPS), elastomeric nitrile rubber (Rubber), and corrugated paper (Paper), are prepared, and these insulations are used to produce mortar specimens with different arrangements. The virtual specimens are designed to evaluate the effect of anisotropic insulations on the material using numerical methods, and the results are adopted to produce real insulating specimens. Low-order probabilistic functions and their modified indexes are utilized for the characterization of the insulation distribution. The physical properties, such as thermal conductivity and compressive strength, are examined using both FE simulations and experimental tools. Then, the correlation between the material characteristics and properties is investigated.

The anisotropy of the insulation distribution is effectively examined using the characterization methods utilized here. Comparing the directional material properties, it is demonstrated that the thermal conductivity is smaller when heat flows in the direction perpendicular to the flat surface of the coin-shaped insulation, while the strength is larger when the loading direction is parallel to the flat surface. Among the three insulation materials used here, EPS is the most effective material to improve the insulation effect, although strength loss should be carefully considered. The results confirm that appropriately arranged anisotropic insulations can be effectively used to obtain a material with low thermal conductivity by minimizing strength loss, and anisotropic insulations/pores can be a promising method for better insulating material without increasing the insulation/pore volume.

Acknowledgements

The project is supported by the German Federal Ministry of Education and Research (BMBF, Project Number: 13XP5010B and 01DR16007) and the German Academic Exchange Service (DAAD, Ref. No.: 91563255). The authors also want to thank Mr. Paul H. Kamm (Helmholtz Centre Berlin) for his assistance in CT imaging.

Open Access

This article is distributed under the terms of the Creative Commons Attribution 4.0 International License (<http://creativecommons.org/licenses/by/4.0/>), which permits unrestricted use, distribution, and reproduction in any medium, provided you give appropriate credit to the original author(s) and the source, provide a link to the Creative Commons license, and indicate if changes were made.

References

- ABAQUS. (2013). Version 6.13, Dassault Systemes, Pawtucket, Rhode Island.
- Baetens, R., Jelle, B. P., & Gustavsen, A. (2011). Aerogel insulation for building applications: A state-of-the-art review. *Energy and Buildings*, *43*, 761–769.
- Benmansour, N., Agoudjil, B., Gherabli, A., Kareche, A., & Boudenne, A. (2014). Thermal and mechanical performance of natural mortar reinforced with date palm fibers for use as insulating materials in building. *Energy and Buildings*, *58*, 98–104.
- Binici, H., Aksogan, O., & Demirhan, C. (2016). Mechanical, thermal and acoustical characterizations of an insulation composite made of bio-based materials. *Sustainable Cities and Society*, *20*, 17–26.
- Cabrillac, R., Fiorio, B., Beaucour, A., Dumontet, H., & Ortola, S. (2006). Experimental study of the mechanical anisotropy of aerated concretes and of the adjustment parameters of the introduced porosity. *Construction and Building Materials*, *20*, 286–295.
- Cabrillac, R., & Malou, Z. (2000). Mechanical modelization of anisotropic porous materials with a homogenization method. Application to aerated concretes. *Construction and Building Materials*, *14*, 25–33.
- Chabannes, M., Benezet, J.-C., Clerc, L., & Garcia-Diaz, E. (2014). Use of raw rice husk as natural aggregate in a lightweight insulating concrete: An innovative application. *Construction and Building Materials*, *70*, 428–438.
- Chung, S.-Y., & Han, T.-S. (2010). Reconstruction of random two-phase polycrystalline solids using low-order probability functions and evaluation of mechanical behavior. *Computational Materials Science*, *49*, 705–719.
- Chung, S.-Y., Han, T.-S., Kim, S.-Y., Kim, J.-H. J., Youm, K. S., & Lim, J.-H. (2016). Evaluation of effect of glass beads on thermal conductivity of insulating concrete using micro CT images and probability functions. *Cement and Concrete Composites*, *65*, 150–162.
- Chung, S.-Y., Han, T.-S., Yun, T. S., & Yeom, K. S. (2013). Evaluation of the anisotropy of the void distribution and the stiffness of lightweight aggregates using CT imaging. *Construction and Building Materials*, *48*, 998–1008.
- Chung, S.-Y., Stephan, D., Elrahman, M. A., & Han, T.-S. (2016). Effects of anisotropic voids on thermal properties of insulating media investigated using 3D printed samples. *Construction and Building Materials*, *111*, 529–542.
- Coker, D. A., & Torquato, S. (1995). Extraction of morphological quantities from a digitized medium. *Journal of Applied Physics*, *77*, 6087–6099.

- DeutscheNorm, Plastics—Determination of thermal conductivity and thermal diffusivity—Part 2: Transient plane heat source (Hot Disc) method, German version EN ISO 22007-2, Berlin, Germany, 2012.
- DeutscheNorm. (2010). *Testing hardened concrete—Part 4: Compressive strength; Specification for testing machines*, German version EN 12390-4:2000, Berlin, Germany.
- Dorey, R., Yeomans, J., & Smith, P. (2002). Effect of pore clustering on the mechanical properties of ceramics. *Journal of the European Ceramic Society*, 22, 403–409.
- Gokhale, A., Tewari, A., & Garmestani, H. (2005). Constraints on microstructural two-point correlation functions. *Scripta Materialia*, 53, 989–993.
- Gunduz, L. (2008). The effects of pumice aggregate/cement ratios on the low-strength concrete properties. *Construction and Building Materials*, 22, 721–728.
- Han, T.-S., & Dawson, P. R. (2005). Representation of anisotropic phase morphology. *Modelling and Simulation in Materials Science and Engineering*, 13, 203–223.
- Hao, J.-H., Chen, Q., & Hu, K. (2016). Porosity distribution optimization of insulation materials by the variational method. *International Journal of Heat and Mass Transfer*, 92, 1–7.
- Incropera, F. P., Dewitt, D. P., Bergman, T. L., & Lavine, A. S. (2006). *Fundamentals of heat and mass transfer*. New York: Wiley.
- Jankowiak, T., & Lodygowski, T. (2008). Identification of parameters of concrete damage plasticity constitutive model. *Foundations of Civil and Environmental Engineering*, 6, 53–69.
- Jiang, D., Cui, S., Song, X., & Zhang, J. (2013). Analysis of micro-morphology and heat-insulating property of leaf concrete. *Construction and Building Materials*, 49, 663–671.
- Ke, Y., Beaucour, A. L., Ortola, S., Dumontet, H., & Cabrillac, R. (2009). Influence of volume fraction and characteristics of lightweight aggregates on the mechanical properties of concrete. *Construction and Building Materials*, 23, 2821–2828.
- Kmieciak, P., & Kaminski, M. (2011). Modelling of reinforced concrete structures and composite structures with concrete strength degradation taken into consideration. *Archives of Civil and Mechanical Engineering*, 11, 623–636.
- Kumar, H., Briant, C. L., & Curtin, W. A. (2006). Using microstructure reconstruction to model mechanical behavior in complex microstructures. *Mechanics of Materials*, 38, 818–832.
- Lu, B., & Torquato, S. (1992). Lineal-path function for random heterogeneous materials. *Physical Review A*, 45, 922–929.
- Narayanan, N., & Ramamurthy, K. (2000). Structure and properties of aerated concrete: A review. *Cement and Concrete Composites*, 22, 321–329.
- Neithalath, N., Sumanasooriya, M. S., & Deo, O. (2010). Characterizing pore volume, size, and connectivity in pervious concretes for permeability prediction. *Materials Characterization*, 61, 802–813.
- Ng, S.-C., & Low, K.-S. (2010). Thermal conductivity of newspaper sandwiched aerated lightweight concrete panel. *Energy and Buildings*, 42, 2452–2456.
- Owrak, M., Aminy, M., Jamal-Abad, M. T., & Dehghan, M. (2015). Experiments and simulations on the thermal performance of a sunspace attached to a room including heat-storing porous bed and water tanks. *Building and Environment*, 92, 142–151.
- Roma Jr., L. C., Martello, L. S., & Savastano, H. (2008). Evaluation of mechanical, physical and thermal performance of cement-based tiles reinforced with vegetable fibers. *Construction and Building Materials*, 22(4), 668–674.
- Russ, A., Schwartz, J., Bohacek, S., Lubke, H., Ihnat, B., & Pazitny, A. (2013). Reuse of old corrugated cardboard in constructional and thermal insulating boards. *Wood Research*, 58, 505–510.
- Sales, A., Souza, F. R., Santos, W. N., Zimer, A. M., & Almeida, F. C. R. (2010). Lightweight composite concrete produced with water treatment sludge and sawdust: Thermal properties and potential application. *Construction and Building Materials*, 24, 2446–2453.
- Tewari, A., Gokhale, A. M., Spowart, J. E., & Miracle, D. B. (2004). Quantitative characterization of spatial clustering in three-dimensional microstructures using two-point correlation functions. *Acta Materialia*, 52, 307–319.
- Wong, R. C. K., & Chau, K. T. (2005). Estimation of air void and aggregate spatial distributions in concrete under uniaxial compression using computer tomography scanning. *Cement and Concrete Research*, 35, 1566–1576.
- Yucel, K., Basyigit, C., Ozel, C. (2003). Thermal insulation properties of expanded polystyrene as construction and insulating materials. In *15th symposium on thermophysical properties* (pp. 54–66).
- Zake-Tiluga, I., Svinka, R., & Svinka, V. (2014). Anisotropy of compressive strength in porous alumina ceramics. *Key Engineering Materials*, 604, 153–156.